Terr. Atmos. Ocean. Sci., Vol. 31, No. 6, 633-648, December 2020 doi: 10.3319/TAO.2020.04.29.01

The role of falling ice radiative effects on climate projections over Arctic under global warming

Jui-Lin Frank Li[1, *], Wei-Liang Lee[2], Kuan-Man Xu[3], Jonathan Jiang[1], Eric Fetzer[1], Chao-An Chen[2], Yi-Hui Wang[4], Jia-Yuh Yu[5], Pei-Chun Hsu[2], and Huang-Hsiung Hsu[2]

[1] *Jet Propulsion Laboratory, California Institute of Technology, Pasadena, CA, USA*
[2] *RCEC, Academia Sinica, Taipei City, Taiwan*
[3] *Science Directorate, NASA Langley Research Center, Hampton, VA, USA*
[4] *California Polytechnic State University, San Luis Obispo, CA, USA*
[5] *Department of Atmospheric Sciences, National Central University, Taoyuan City, Taiwan*

Article history:
Received 4 August 2019
Revised 19 April 2020
Accepted 29 April 2020

Keywords:
GCM, Arctic sea ice, Falling ice, Radiation, Warming climate

Citation:
Li, J.-L. F., W.-L. Lee, K.-M. Xu, J. Jiang, E. Fetzer, C.-A. Chen, Y.-H. Wang, J.-Y. Yu, P.-C. Hsu, and H.-H. Hsu, 2020: The role of falling ice radiative effects on climate projections over Arctic under global warming. Terr. Atmos. Ocean. Sci., 31, 633-648, doi: 10.3319/TAO.2020.04.29.01

ABSTRACT

Most global climate models, such as CMIP5 models, ignore the falling ice (snow) radiative effects (FIREs). Extended from our previous works, we explore the impacts of FIREs on the geographical distribution changes of sea ice concentration (SIC), sea ice thickness and skin temperature (Ts) under 1% per year increase of atmospheric CO_2 concentration. We perform a pair of 140-year experiments including FIREs (SoN) and excluding FIREs (NoS) using CESM1-CAM5. These two simulations are compared with each other and against CMIP5 multi-model mean without FIREs (CMIP5-NoS). The results show that the changes of SIC, thickness and radiation fields in NoS minus SoN largely match the changes between CMIP5-NoS and SoN in winter but less so in summer and annual mean. Both NoS and CMIP5-NoS simulate less downward longwave and net radiative warming (~20 - 30 W m^{-2}), resulting in colder Ts over Arctic and adjacent lands (~5 - 8 K colder) and stronger meridional temperature gradient, leading to more SIC and thicker sea ice (~30 - 40 cm) over the Arctic ocean. The inclusion of FIREs produces stronger changes in geographic patterns and magnitudes of Ts, SIC and thickness from the first to middle 20 years but less from the middle to last 20 years. The SIC and thickness changes in SoN are associated with warmer Ts, increasing downward surface longwave warming and thus net warming relative to NoS and CMIP5-NoS. With FIREs, the model shows faster warming-driven sea ice retreats and thinning over the entire Arctic ocean, resulting in a sea ice-free Arctic ocean 30 years earlier, as well as much warmer Ts (up to 5 K) over the adjacent lands than in NoS case.

1. INTRODUCTION

The Arctic oceans and adjacent lands are becoming warmer (Boisvert and Stroeve 2015) along with melting sea ice, land ice melting (Jacob et al. 2012; Kjeldsen et al. 2015) and model projected land degradation of permafrost affecting the structural integrity of infrastructure (Shiklomanov et al. 2017). The melting Arctic sea ice results in more open oceans that may decrease local surface albedo (Smith and Stephenson 2013), affect energy and moisture exchanges and radiation balance at the top of atmosphere (Tietsche et al. 2011; Bintanja and Selten 2014). The faster melting Arctic sea ice associated with rapidly warmed surface and lower atmosphere has profound impacts on inhabitants of the Arctic region and surround areas. For example, the warmer Arctic and its adjacent areas reduce the meridional and latitudinal temperature gradient weakening the upper-level jets, resulting in more frequent extreme weather events at mid-high latitudes (Francis and Vavrus 2012). However, the causality between the Arctic changes and the jet-stream and thereby influence weather patterns farther south is still an open question (Barnes and Screen 2015).The sea ice extent minima in 2007 and 2012 are related to the rapid retreat of Arctic sea ice due to the surface energy changes caused

* *Corresponding author*
E-mail: jli@jpl.nasa.gov

by anomalous cloud cover reduction resulting in sea ice thickness thinning (Kay et al. 2008) and atmospheric and oceanic circulation exporting sea ice to out of Arctic oceans (Smedsrud et al. 2017).

To explore the above-mentioned sea ice variations, global climate models (GCMs) such as those participated in the fifth phase of Coupled Model Intercomparison Project (CMIP5, Taylor et al. 2012) models are commonly used. These models show that the observed sea ice retreating and extreme low sea ice have been attributed to wind-driven sea ice advection (Rigor and Wallace 2004), global warming and natural variability (Kay et al. 2011; Kirchmeier-Young et al. 2017).

It is essential to understand the above-mentioned physical and dynamical processes that are responsible for sea ice and adjacent land skin temperature changes for future projections needed by policy decision makers. In particular, it is critical to project the time for an "ice free" Arctic, if it would occur, and the speed of sea ice melting under various anthropogenic warming scenarios. So far, the projections with GCMs are not yet reaching a general consensus (Massonnet et al. 2012; Stroeve et al. 2012). For example, under anthropogenic warming scenario experiments projected in CMIP5, the ice free time reported in Massonnet et al. (2012) is in 2041 - 2060, while in Stroeve et al. (2012) it is suggested that it would be in next few decades.

The lack of a general consensus may be related to accurate representation of relevant physics. Li et al. (2019) highlighted the role of falling ice (snow) radiative effects (FIREs) in simulating the time series of the Arctic sea ice variations. The observed sea ice variations such as faster melting and slower formations are not simulated by the multi-model-mean (MMM) and most individual CMIP5 GCMs due to the lack of FIREs. Over the Antarctic, Li et al. (2017) found that the FIREs are more important for the winter seasons and annual mean state in present-day scenario (historical run in CMIP5) mainly because with the inclusion of two third of falling ice mass increases, the downward longwave heating on the sea ice areas increases, which in turn restricts sea-ice growth while there is no solar radiation during winter. Over the Arctic, the wintertime sea ice extent might be restricted by adjacent lands and thicker sea ice; i.e., the mean thickness of 3 - 4 m compared to Antarctic of 2 - 3 m (Kwok and Cunningham 2008; Kurtz and Markus 2012).

There are many studies using the CMIP5 model output to examine projected sea ice changes and associated physical-dynamical processes (e.g., Cesana et al. 2012, 2015; Karlsson and Svensson 2013; Koenigk et al. 2014; Tan et al. 2016; Horvat and Tziperman 2018; Massonnet et al. 2018). As a summary, sea ice changes could be affected by complex physical-dynamical processes, for example, any process that affects the baseline thickness leading to future retreat, ocean eddy heat flux and cloud schemes that affect surface radiation and temperature change, as well as treatment of the mixed phase clouds. Differences in atmospheric, ocean and sea ice components among CMIP5 models may cause complex changes in sea ice. In this study, we will use CMIP5 outputs to determine whether differences in projected sea ice can be detected between models with FIREs and non-FIREs. We will focus on this physical process using controlled Community Earth System Model version 1 with the Community Atmosphere Model version 5 (CESM1-CAM5) simulations with and without FIREs, which allows for a direct detection of our FIREs hypothesis.

This study extends from Li et al. (2019) but focuses on the Arctic and adjacent lands. We attempt to quantify the impacts of FIREs on the geographic distribution changes of projected Arctic sea ice and land skin temperature and relationships with surface radiation budget under global warming. We discuss how the inclusion of FIREs (SoN), compared to without (SoN), can substantially change simulated Arctic sea ice extent and sea ice thickness and where the geolocation of changes is under global warming. We present the results in terms of annual mean and seasonal changes of SIC, THK and radiation fields in NoS minus SoN with warming climate, compared with those of CMIP5 without FIREs (CMIP5-NoS) minus SoN.

In section 2, we describe the controlled simulations and analysis methods. Results are presented in section 3. We discuss and conclude major findings in section 4.

2. METHODS

2.1 Controlled Climate Model Simulations

Following the CMIP5 1%CO2 protocol, the climate change simulations are initialized from a preindustrial control (piControl) run with an increase in atmospheric CO_2 at 1% yr^{-1} for 140 years. We perform a pair of simulations with FIREs on (SoN) and off (NoS) using the National Center for Atmospheric Research-Department of Energy (NCAR-DOE) CESM1-CAM5. The model is composed of the Earth's atmosphere, ocean, land surface, and sea-ice. Model codes and documentation are available at http://www.cesm.ucar.edu/models/cesm1.0/. We only provide a brief description of the cloud microphysics parameterization used in CESM1-CAM5 here.

The Morrison-Gettelman scheme is a four-class (liquid, ice, rain, and snow), two-moment cloud microphysics, as described in Morrison and Gettelman (2008), which is used to represent stratiform clouds and precipitation. It includes the diagnosis of falling ice mass flux at each model level at each model physical time step (Morrison and Gettelman 2008; Gettelman et al. 2010). Falling ice (snow) in the model represents falling large ice crystals with appreciable falling velocities, whose radiative effects are considered (Gettelman et al. 2010), using the diagnosed mass and effective radius of falling snow crystals (Morrison and Gettelman 2008). The snow particle shape recipe was based on

the crystal shape observations at -45°C: 7% hexagonal columns, 50% bullet rosettes, and 43% irregular ice particles. The simulated cloud ice and snow are comparable to the CloudSat retrieval (Gettelman et al. 2010). Further details regarding the diagnosed snow mass is described in Morrison and Gettelman (2008) and its radiative properties in CAM5 are provided in Gettelman et al. (2010). Note that the diagnostic snow is for stratiform grid-scale clouds while the subgrid-scale convective "floating" cloud ice and liquid are diagnosed and used for radiative transfer in a very simple form. The convective snow, however, is not yet included in the version of NCAR CAM5 used in this study (Gettelman and Morrison 2015; Gettelman et al. 2015).

2.2 Analysis Method

The surface energy balance and its connection with surface skin temperatures (Ts) and other cryosphere parameters, including sea ice concentration (SIC), thickness (THK) and snow on sea ice area (SNOW) are analyzed following the method in earlier studies (Li et al. 2017, 2019).

The magnitudes of the area-averaged (over 60 - 90°N ocean only; including sea ice coverage) surface downward shortwave flux (RSDS), surface downward longwave flux (RLDS) and reflected shortwave flux (RSUS) are much larger than those of latent heat flux (LHF: ~10 - 20 W m^{-2}) and sensible heat flux (SHF: ~2 - 15 W m^{-2}) (figures not shown). That is, the effects of LHF and SHF are negligible compared to net radiation contributions (~100 - 300 W m^{-2}). By assuming a small net heat uptake or release from the surface, which is a good approximation for studying non-transient behavior (20-year average, in this study), the surface energy budget may be written as:

$$\epsilon\sigma T_s^4 \cong RLDS + RSDS - RSUS \quad (1)$$

where ϵ is the surface emissivity, σ the Stefan-Boltzmann constant, T_s the surface skin temperature. The combination of the three radiative fluxes on the right-hand-side of Eq. (1) is for the response of surface thermal emission, that is, $RLUS = \epsilon\sigma T_s^4$, which can be called "approximated net input flux for surface emitting longwave radiative flux" (referred as AELW) or "net radiative flux (Net)" with respect to the net surface radiative flux and the response to the atmospheric radiative flux input for short. Interested readers may refer to Li et al. (2017, 2019) for more details.

We analyze two 1%CO2 simulations with CESM1-CAM5, and refer to these simulations as SoN (FIREs on) and NoS (FIREs off). In addition, twelve CMIP5 models (without FIREs included) with 1%CO2 simulations are considered (Table 1), and their ensemble mean (CMIP5-NoS) is compared against NoS and SoN. Note that none of 12 CMIP5 models includes FIREs except for CESM1-CAM5.

We found that the results are insensitive to the length of averaging periods of 10 - 30 years, and we thus present 20-year averages here for three warming stages: "initial" for years 1 - 20 (first 20 years), "middle" for years 61 - 80 (middle 20 years), and "warmest" for years 121 - 140 (last 20 years). Li et al. (2019) showed that present-day radiative flux and sea ice biases are reduced when including FIREs as in SoN. We also examine the climate change tendency component by subtracting the mean of years 1 - 20 (first 20) from that of years 121 - 140 (last 20), and denoted this as $()'$. The difference in simulated climate change due to FIREs is the difference between the SoN and NoS experiments for the change between two climates, which is donated as $\delta()'$.

Table 1. A list of 12 coupled atmosphere-ocean climate models in CMIP5 archive under 1%CO2 used in this study.

Model	Description
ACCESS1-3	Commonwealth Scientific and Industrial Research Organisation, and Bureau of Meteorology (Australia)
BCC-CSM1-1	Beijing Climate Center, China Meteorological Administration (China)
BCC-CSM1-1-m	Beijing Climate Center, China Meteorological Administration (China)
BNU-ESM	College of Global Change and Earth System Science, Beijing Normal University (China)
CanESM2	Canadian Centre for Climate Modelling and Analysis (Canada)
CCSM4	National Center for Atmospheric Research (USA)
CNRM-CM5	Centre National de Recherches Meteorologiques / Centre Europeen de Recherche et Formation Avancees en Calcul Scientifique (France)
IPSL-CM5A-LR	Institut Pierre-Simon Laplace (France)
MIROC-ESM	Japan Agency for Marine-Earth Science and Technology, Atmosphere and Ocean Research Institute (The University of Tokyo), and National Institute for Environmental Studies (Japan)
MPI-ESM-LR	Max Planck Institute for Meteorology (MPI-M) (Germany)
MRI-CGCM3	Meteorological Research Institute (Japan)
NorESM1-ME	Norwegian Climate Centre (Norway)

We examine geographical distributions (maps) over 40 - 90°N so that the majority of the sea ice and adjacent land areas are included. While the average for time series over 70 - 90°N is used for sea ice to minimize differences due to inconsistent land-sea masking between CMIP5 models. For CESM1-CAM5 the average over 60 - 90°N is used to see the general impacts of the FIREs. For all simulations, we examine surface radiative energy budget components: upward and downward shortwave and downward longwave fluxes, as well as surface skin temperature (including land) and sea ice thickness (THK) and sea ice concentration (SIC).

3. RESULTS

3.1 Impacts of FIREs on Changes of Annual-Mean Climatology for Three Stages

Figure 1a shows the time series of ocean-only area averages of monthly SIC values from NoS, SoN and CMIP5-NoS over the belts 70 - 90°N. For time series of single-month (March and September) SIC and CMIP5-NoS intermodel variability of SIC, see Li et al. (2019) and Supplementary Information Fig. S1. The impact of FIREs seems to be small initially and then increases gradually with time. For example, the SIC in NoS and CMIP5-NoS is slightly higher than SoN in the first 40 years and then becomes higher in years 40 - 90 and in the last 20 years (years 120 - 140) with differences of 10 - 25%. Similar to SIC, the surface AELW (net flux) and skin temperature (Ts) show similar trends (Figs. 1b and c) with differences of 5 - 20 W m^{-2} and 2 - 5 K, respectively. Interestingly, the overall trends of SIC, net flux and Ts start to diverge between NoS (and CMIP5-NoS) and SoN at approximately year 40 with an oscillatory behavior in the middle period. In general, SIC decreases and surface temperature warms with time more rapidly when FIREs are included, due to stronger downward net flux. The stronger radiative heating and warmer surface air reinforces Arctic sea ice retreat.

Same as in Fig. 1 but for NoS and SoN only, Fig. 2 shows the annual-mean (ANN: Figs. 2a - c) and seasonal-mean (DJF, Figs. 2d - f; MAM, Figs. 2g - i; JJA, Figs. 2j - l; SON, Figs. 2m - o) variations of area-averaged SIC, snow on sea ice area (SNOW) and sea ice thickness (THK) over the belts 60 - 90°N. Similar to Fig. 1, the impacts of FIREs on SIC are small between years 1 - 40 and become significant at the starting point of divergence between SoN and NoS except for the melting seasons in JJA (Fig. 2j) and SON [Fig. 2m; see Li et al. (2019) for September only] which starts to diverge at year 10. In years 40 - 90, SIC is much higher in NoS than in SoN except for the (MAM) frozen season (Fig. 2g). After year 100, SICs of NoS and SoN differ less for all seasons except in DJF (Fig. 2d), when differences are up to 15 - 20% between years 120 and 140. There is no apparent difference in snow on sea ice area (SNOW) for annual and seasonal means between NoS and SoN (Figs. 2b, e, h, k, n).

The impacts of FIREs on THK occur initially at year 5 with 0.2 - 0.3 m thicker in NoS than in SoN, suggesting that part of the longwave warming dominated AELW in SoN is used to thin sea ice at the initial warming stage. The thinning is getting larger between years 40 and 100 with amplitudes up to 0.6 m at year 60. However, THK differences become smaller between NoS and SoN as the climate continues to warm, which strongly impacts the formation/melting of sea ice due to the thinner sea ice. Note that the THK during the melting season reaches nearly zero for SoN at year 70, which is ~30 years ahead of NoS at year 100 (Fig. 2o).

Based on the results presented in Figs. 1 and 2, we examine three stages of the geographical distribution of changes in search of coherent relationships among radiation (RLDS and net flux), Ts, SIC, and THK. Such coherent relationships may not exist over all Arctic seas and can be contributed by other physical-dynamical processes and feedbacks (e.g., Mori et al. 2019), addition to FIREs.

Initial stage: Figures 3a - e show the geographical distribution of the impacts of FIREs on the initial 20-year mean state of RLDS, AELW (Net), Ts, SIC, and THK. Relative to the SoN simulation, with slight changes in SIC (from 2 to 5%; Fig. 3d), the NoS simulation generates much less AELW (from -10 to -15 W m^{-2}; Fig. 3b) in conjunction with colder Ts (from -2 to -3 K; Fig. 3c) over three regions

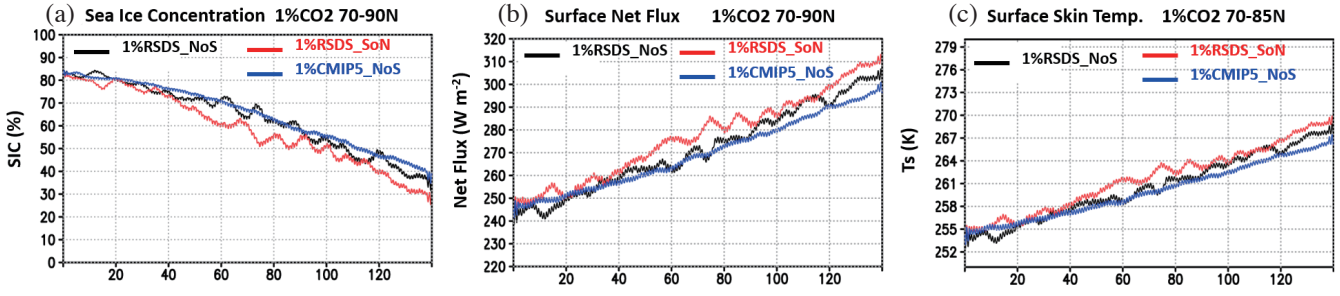

Fig. 1. Ocean only monthly mean time series of (a) sea ice concentration (%) for falling ice radiative effects (FIREs) off (NoS: black line), FIREs on (SoN: red line), and CMIP5 multi-model mean (CMIP5-NoS) without FIREs averaged over the latitude belts 70 - 90°N under 1%CO2 per year for 140 years. (b) Same as (a) but for surface net flux (W m^{-2}); (c) same as (a) but for surface skin temperature (K).

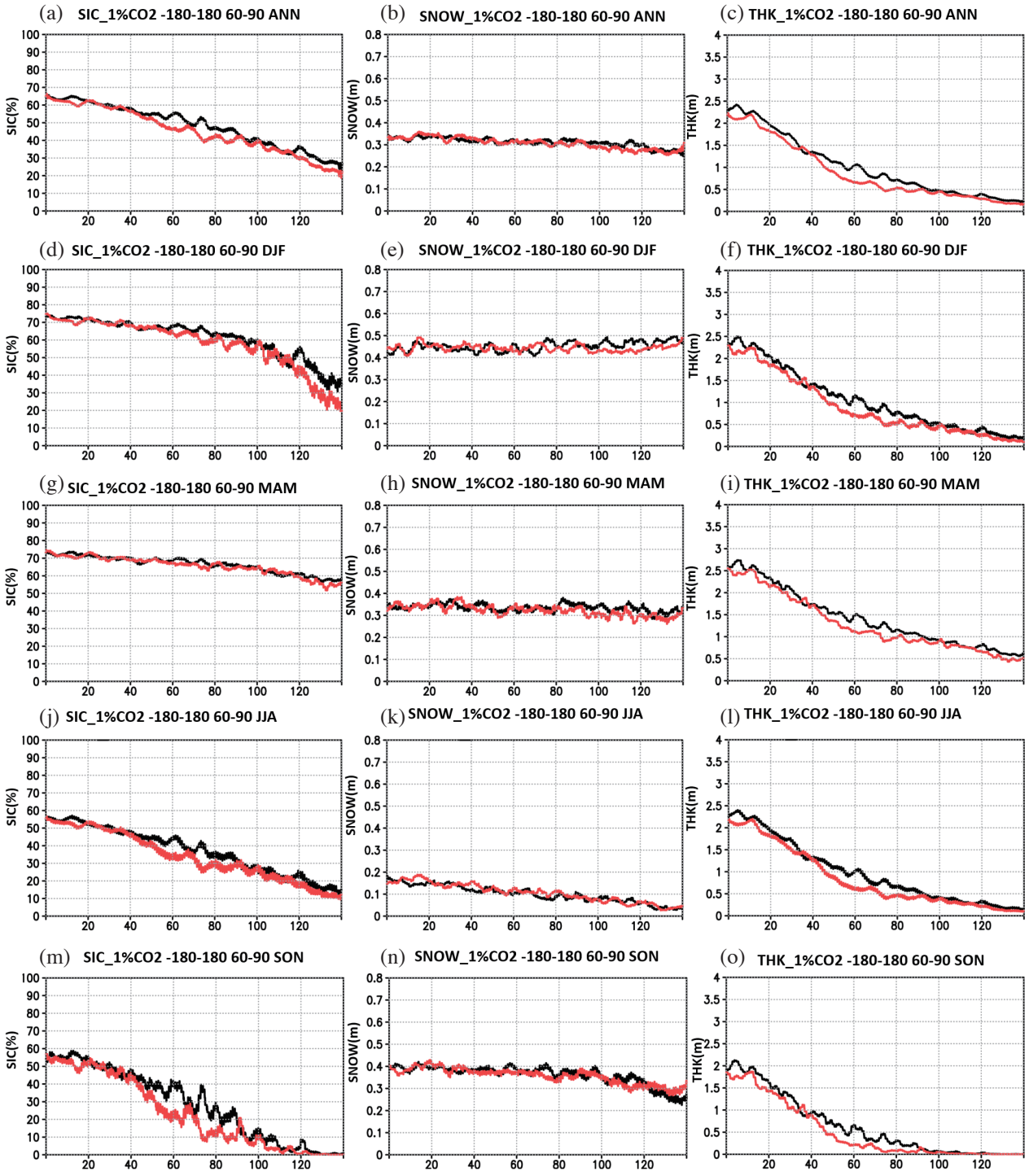

Fig. 2. (a) Ocean only monthly mean time series of sea ice concentration (SIC: %) for falling ice radiative effects (FIREs) off (NoS: black line) and FIREs on (SoN: red line) averaged over the latitude belts 60 - 90°N under 1%CO2 per year for 140 years. (b) Same as (a) but for snow on sea ice area (SNOW: m); (c) same as (a) but for sea ice thickness (THK: m). (d) - (f) Same as (a) - (c) but only for mean December-January-February (DJF). (g) - (i) Same as (a) - (c) but for mean season of March-April-May (MAM). (j) - (l) Same as (a) - (c) but for June-July-August (JJA). (m) - (o) Same as (a) - (c) but for September-October-November (SON).

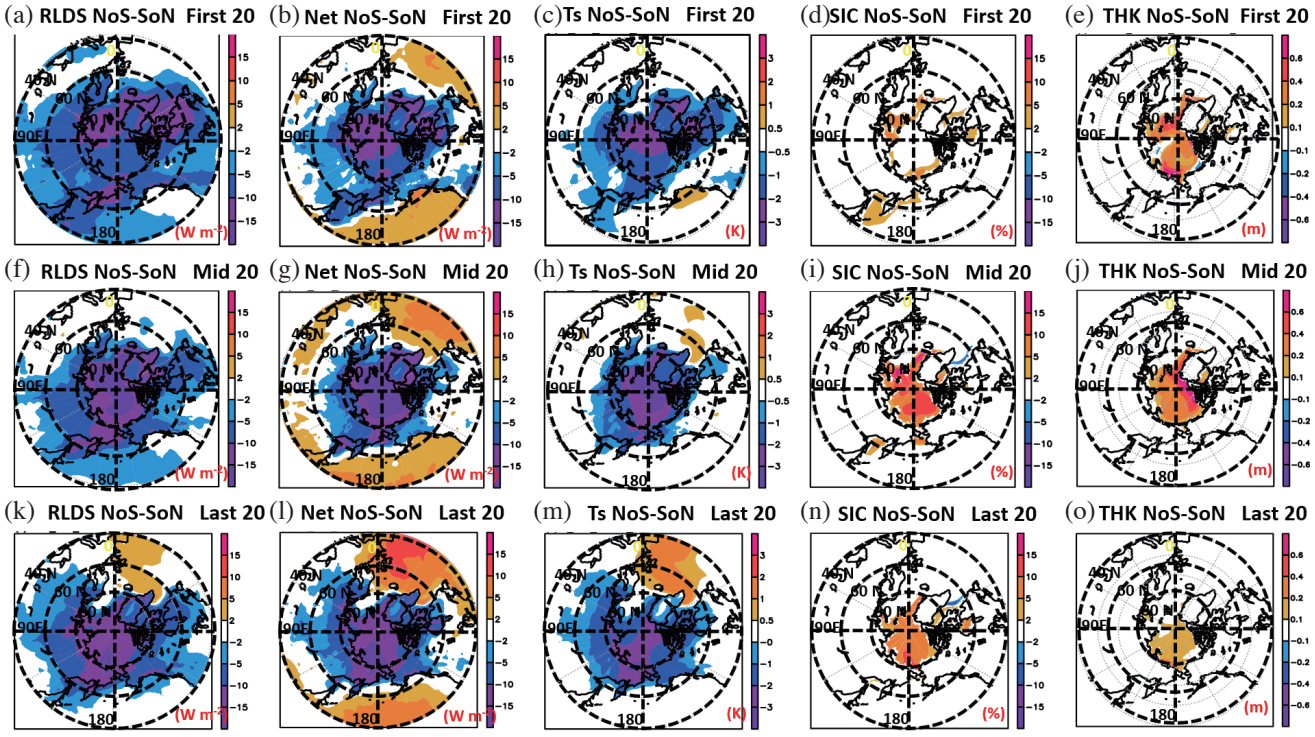

Fig. 3. The difference between falling ice radiative effects (FIREs) on and off (NoS - SoN) annual mean from the first 20 years (1 - 20 years) for (a) surface downward longwave radiation (RLDS: W m^{-2}), (b) same as (a) but for surface net flux (Net: W m^{-2}), (c) same as (a) but for surface skin temperature (Ts: K), (d) same as (a) but for sea ice concentration (SIC: %), (e) same as (a) but for sea ice thickness (THK: m). (f) - (j) Same as (a) - (e) but for the annual mean from the middle 20 years (61 - 80 years). (k) - (o) Same as (a) - (e) but for the annual mean from the last 20 years (121 - 140 years). The NoS and SoN are from CESM1-CAM5 experiments following the CMIP5 1%CO2 scenario for 140 years.

near the edges of North Alaska, the east and west coasts of Greenland associated with thicker THK (from 0.4 to 0.8 m; Fig. 3e) over the entire Arctic oceans.

Middle stage: It is evident that the spatial patterns of RLDS (Fig. 3f) and AELW (Fig. 3g) and Ts (Fig. 3h) over the entire Arctic oceans (north of 82°N) maintain the similar differences at this stage with the magnitudes of differences being amplified in SIC (> 15%; Fig. 3i) with slightly thicker sea ice (Fig. 3j), in particular, over the north Greenland and its west, compared to the initial 20-year mean state. These larger differences are associated with slightly colder Ts (by < -3 K), less AELW (< -15 W m^{-2}) over the same region, compared to SoN. Note that the negative ALEW area is larger than negative Ts area. The latter is larger than the positive SIC and THK areas. This suggests that other physical-dynamical processes may play more important roles over the lower latitudes, in addition to FIREs.

Warmest stage: In the last 20 years, the spatial patterns of RLDS (Fig. 3k) and AELW (Fig. 3l) and Ts (Fig. 3m) over the entire Arctic oceans north of 82°N maintain the similar differences with the magnitudes of differences being smaller in SIC (~10%; Fig. 3n) and THK (~0.2 m; Fig. 3o), in particular, over the north Greenland and its west, compared to the middle 20-year mean state. These differences are associated with slightly colder Ts (by < -2 K) and less AELW (< -10 W m^{-2}) over the same region, compared to SoN. The impacts on the north-south Ts gradient are enhanced over north Atlantic Ocean between 60 and 80°N, indicating enhancement of north-south sea surface temperature gradients with potential change in ocean circulations. Colder land Ts are found over 60°N over Asia and North America in NoS. These Ts gradient changes may change atmospheric circulations and cause more extreme weather events at mid-high latitudes (Francis and Vavrus 2012).

Shown in Appendix, Figs. A1 and A2 show the significant levels ($p < 0.05$) for the changes in radiation fields, Ts and SIC and THK for DJF (Fig. A1) and JJA (Fig. A2) from year 1 to 140 years. The stippled areas indicating the changes are all significant for RLDS in DJF (Fig. A1) and RSDS/RSUS in JJA (Fig. A2) leading to the changes in skin temperature and SIC and thickness. Given the aforementioned differences in 140 years of surface radiative fluxes, Ts and SIC between NoS and SoN, we primarily discuss three stages of the 140-year simulations, proposing a mechanism explaining progressive changes from the initial toward warmer climates as follows: models excluding FIREs produce colder Ts, which lead to increases in SIC and sea ice thickness relative to those with FIREs. The colder Ts is due to less AELW (heating) that is contributed mainly from reducing surface downward longwave, and

increasing summer (JJA) surface downward shortwave flux (Figs. A3c - A5c) and their counteracting (cooling) upward shortwave fluxes (up to 15 - 20 W m^{-2}) (Figs. A3f - A5f).

3.2 Impacts of FIREs on Seasonal Surface Energy Budget, Sea-Ice Concentration, Thickness, and Snowfall

To further qualify the impact of FIREs on progressive warmer climates at three stages, we present NoS minus SoN results for summer, June-July-August (JJA) and winter, December-January-February (DJF).

Same as in Fig. 3, the DJF season is shown in Fig. 4. The spatial patterns of RLDS and AELW over the entire Arctic are amplified for all three stages (< 15 - 25 W m^{-2}) compared to other seasons (not shown). The associated skin temperatures are getting much colder in winter from initial to the warmest stages. In particular, in the last 20 years, much colder land Ts (from 3 to 8 K; Fig. 4m) expands into Asia and North America north of 60°N, resulting from less RLDS (Fig. 4k) and AELW (Fig. 4l). That is to say, the model's Ts would be several degrees higher when the FIREs are included. The differences in SIC and THK of a progressive warmer climate are similar to those of the annual means shown in Figs. 3d, i, and n in SIC except in the last 20 years when the SIC is much larger in NoS than in SoN, which can be up to 15 - 30% (Fig. 4n).

These differences are found not only over the Arctic oceans but also over all mid- and high-latitude continental regions during the winter season (DJF). Interestingly, models including FIREs would produce stronger RLDS and AELW warming (15 - 25 W m^{-2}), resulting in much warmer Ts (by 3 - 8 K), compared to NoS in the last 20 years. The impacts of FIREs on the north-south Ts gradient over west Europe reach the maximum in the middle 20 years while over Atlantic oceans they shift closer to the Arctic oceans between 60 and 80°N, indicating weaker north-south sea surface temperatures gradients over Atlantic Ocean.

Same as in Fig. 3 except for adding shortwave radiative budget components [Eq. (1)], the progressive climate changes of the NoS minus SoN maps in summer (JJA) for three stages are shown in Fig. 5. Under the initial warming stage, NoS produces colder Ts (up to -1 to -2 K) over Arctic near the pole with less RLDS (5 - 10 W m^{-2}) and decreasing net flux (10 - 15 W m^{-2}) than the SoN simulation. From the initial to last stages, NoS produces stronger surface albedo cooling (Figs. 5c, j, q), offsetting more downward solar radiation (Figs. 5b, j, p). The former contributes greatly to the net surface cooling there (Figs. 5d, k, r). The summer sea ice formation is stronger during the middle to last 20 years (Figs. 5m, t) in NoS over the entire Arctic area. Amplification of sea ice formation due to RLDS and RSUS cooling increases the differences in THK (Figs. 5g, n) between NoS and SoN up to 40 - 60 cm, but at the last stage the THK differences (Fig. 5u) are smaller in areas with small Ts differences, which is related to the smaller mean sea-ice thicknesses at end of both simulations (Fig. 2l).

In summary, without FIREs, from the initial to warmest climate, during winter (DJF) when solar radiation contributes little to the net flux changes (Figs. A3 - A5), the changes in the net flux are becoming dominated by less downward LW radiation, leading to broader regions (including lands) of colder Ts with more sea ice concentration, along with thicker sea ice over sea ice regions. Over parts of the lower-latitude oceans, there are larger areas of warmer Ts, compared to the annual mean, associated with increasing net flux. The enhancement of south-north Ts gradients might have important implications for ocean circulations and atmospheric dynamics. For summer, Fig. 5 shows that the relationship between radiative flux and SIC changes is complex due to competition between downward (RSDS) and upward surface shortwave (RSUS) and downward surface longwave radiation (RLDS). In some regions such as over Arctic oceans, there is an increase in downward shortwave radiation (heating) as sea surface temperatures increase but it is offset by RLDS and RSUS (cooling). While over the mid- and high-latitudes land, the net flux increase depends on the competition between RLDS and RSDS as differences in surface shortwave reflection are small between NoS and SoN. Over the Arctic oceans, the sea ice albedo cooling increases along with an increase in sea-ice concentration and thickness when FIREs are excluded (NoS). This seasonal change indicates that the combination of small increases in longwave surface heating with large net SW cooling help with sea-ice growth with thicker sea ice, which leads to a higher surface albedo. This increased cooling by increased albedo is large enough to offset the reduction in longwave heating and downward shortwave at the surface, resulting in summertime sea ice growth in the NoS simulation.

The discussion above illustrates that the SoN simulation produces consistently higher downward surface radiative fluxes and less sea ice concentration with thinner sea ice in a progressive warming climate over Arctic oceans than the NoS simulation. FIREs are contributed by increasing the downward longwave heating in winter, which reduces SIC. In summer, FIREs are contributed by the shortwave reflection over the same region, but reduced albedo could restrict sea-ice growth with warmer Ts due to the increased net radiative heating. This substantially reduces the formation of sea ice relative to the NoS simulation.

3.3 Comparisons with CMIP5 Models

The credential of using NCAR CESM1-CAM5 with SoN relative to NoS in annual-mean, annual cycle and long-term sea ice melting trends from present-day towards warming climate over Arctic oceans was highlighted in Li et al. (2019). In this study, we use SoN as a reference for

comparisons between NoS and CMIP5-NoS by showing geographic distributions of climate changes in details. The results are shown in Fig. 6 for the differences for winter (DJF) between the last and first 20 years periods, representing the climate change between two periods (see section 2.2). The annual-mean and summer climatology are shown in Figs. A6 and A7.

Shown in Fig. 6, in DJF, the distributions of NoS minus SoN climate changes, i.e., the last 20-year minus first 20 years of (NoS - SoN) of RLDS, AELW (Net), Ts and SIC (Figs. 6a - d) are very similar to those in CMIP5-NoS minus SoN (Figs. 6e - h) except for opposite tendency of changes over far north-east Pacific Ocean regions. It is important to point out that both NoS and CMIP5-NoS project higher cooling tendency (magnitudes of ~3 - 8 K) over Europe, north of 40°N, between longitudes of 30 - 90°E.

The annual mean climate changes of each of the four radiative flux components (surface downward SW, LW, and SW reflection to surface net flux; Fig. A6) are generally similar between NoS minus SoN and CMIP5-NoS minus SoN, but with a large disparity in AELW. Also, the summer (JJA) seasonal climate changes in CMIP5-NoS minus SoN (Fig. A7) are very different compared to the differences between NoS and SoN with broader covered regions than NoS minus SoN. The above broader regions disparities seem to be the product of ensemble average resulted from large model spread in simulating the regional characteristics of progressive climate changes among CMIP5 models (Li et al. 2017, 2019). In addition, differences in model physical processes other than FIREs may contribute to the large model spread. The lack of natural variability for single realization of CESM1-CAM5 simulations may be another factor.

The ocean-only area averages of SIC values over the belts 60 - 90°N shown in Figs. 1 and 2 indicate that, during melting seasons, the CESM1-SoN simulation shows a faster long-term sea ice melting rate than the CESM1-NoS without changes in snow on sea ice area, which can be found in the geographical distribution from initial to warmest stages (figures not shown).

4. DISCUSSION AND CONCLUSIONS

We examined the impacts of falling ice (snow) radiative effects (FIREs) on geographical distribution changes of sea ice concentration, sea ice thickness and skin temperature, following a highlight reported in Li et al. (2019). Most of the GCMs participated in CMIP5 do not include FIREs for climate projection. The inclusion of FIREs is one of the important contributions in reducing mean-state and seasonal mean biases in terms of radiation, surface skin temperatures, and sea ice concentration and thickness of the Arctic Ocean both in CESM1 and CMIP5-MMM (Li et al. 2019). In this study, we enabled FIREs (SoN) or disabled FIREs (NoS) in the CESM1-CAM5 fully-coupled runs, which follow the CMIP5 1%CO2 scenario protocol. We have used a similar methodology as in Li et al. (2017, 2019) to assess, in

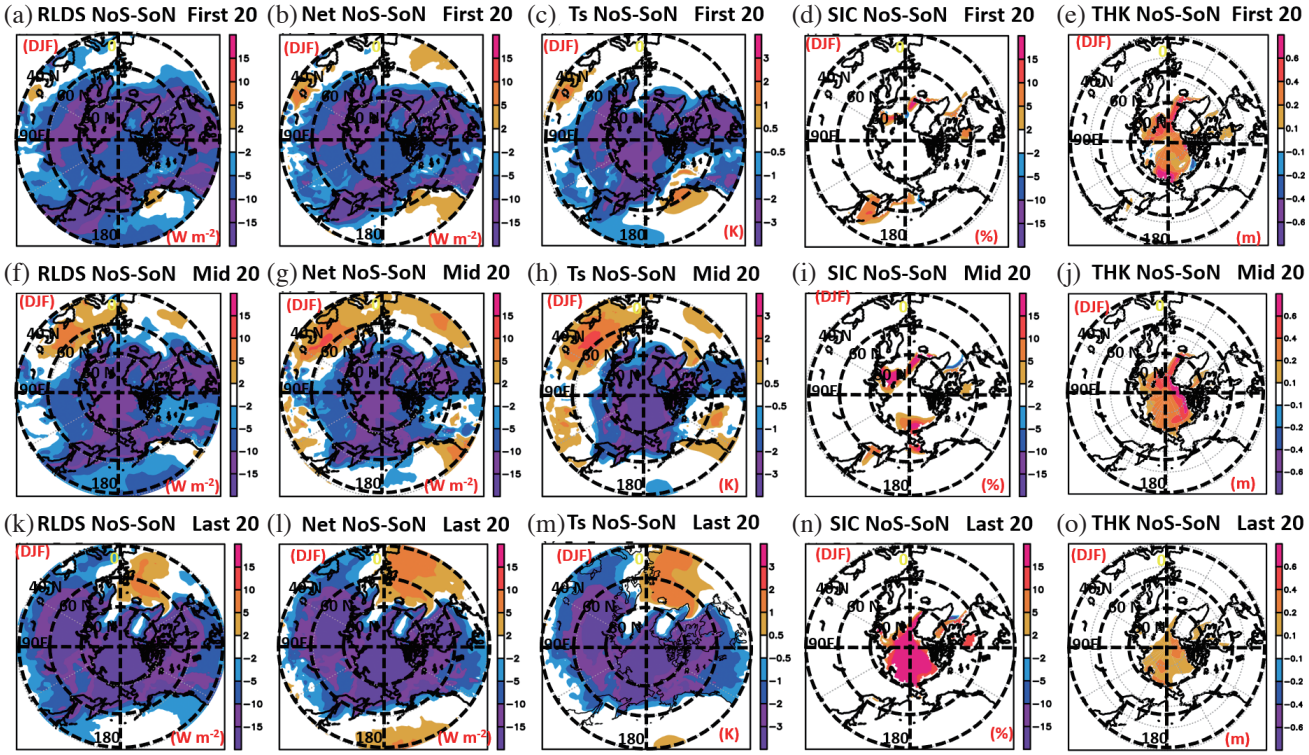

Fig. 4. Same as in Fig. 3 but for mean from December-January-February (DJF) only.

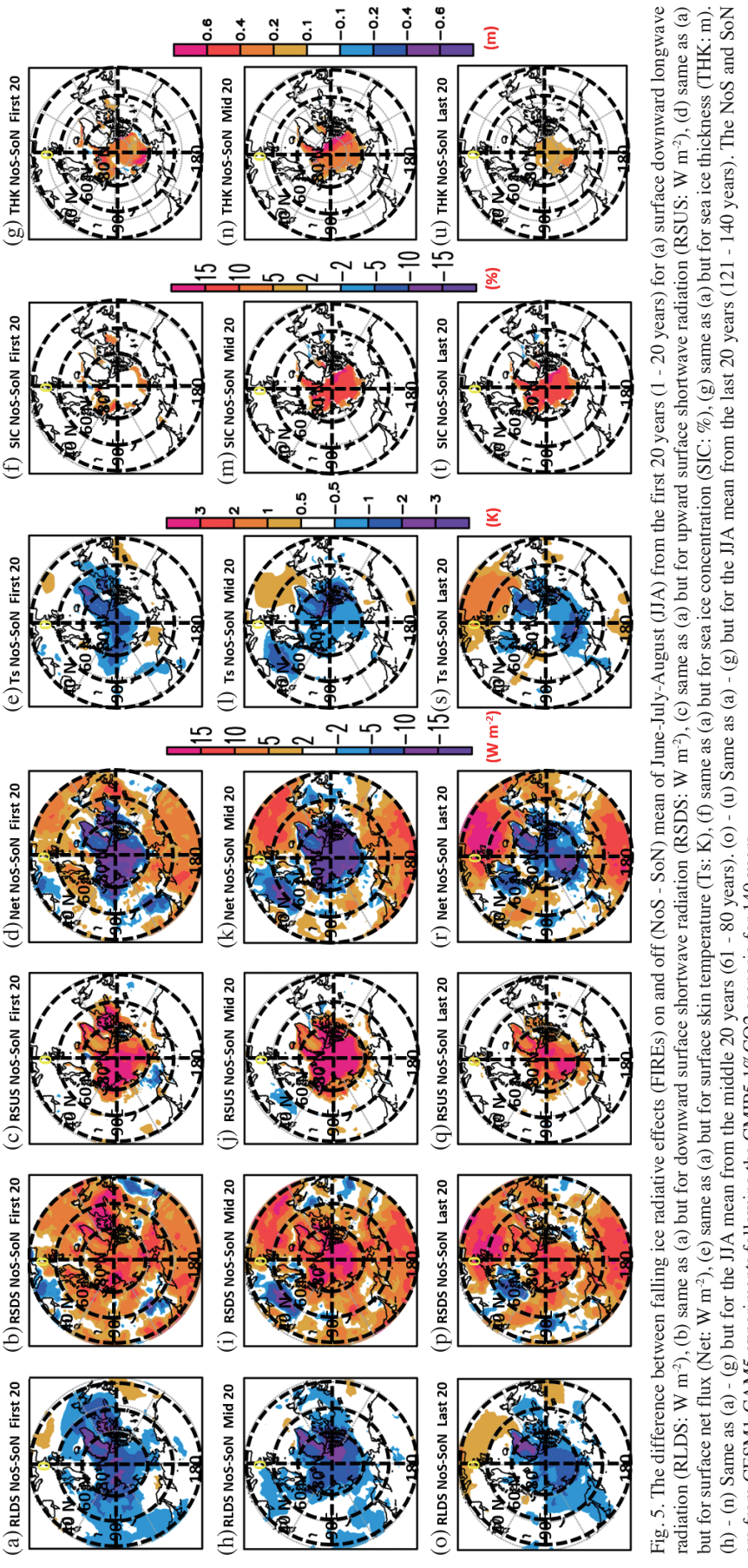

Fig. 5. The difference between falling ice radiative effects (FIREs) on and off (NoS - SoN) mean of June-July-August (JJA) from the first 20 years (1 - 20 years) for (a) surface downward longwave radiation (RLDS: W m^{-2}), (b) same as (a) but for downward surface shortwave radiation (RSDS: W m^{-2}), (c) same as (a) but for upward surface shortwave radiation (RSUS: W m^{-2}), (d) same as (a) but for surface net flux (Net: W m^{-2}), (e) same as (a) but for surface skin temperature (Ts: K), (f) same as (a) but for sea ice concentration (SIC: %), (g) same as (a) but for sea ice thickness (THK: m). (h) - (n) Same as (a) - (g) but for the JJA mean from the middle 20 years (61 - 80 years). (o) - (u) Same as (a) - (g) but for the JJA mean from the last 20 years (121 - 140 years). The NoS and SoN are from CESM1-CAM5 experiments following the CMIP5 1%CO2 scenario for 140 years.

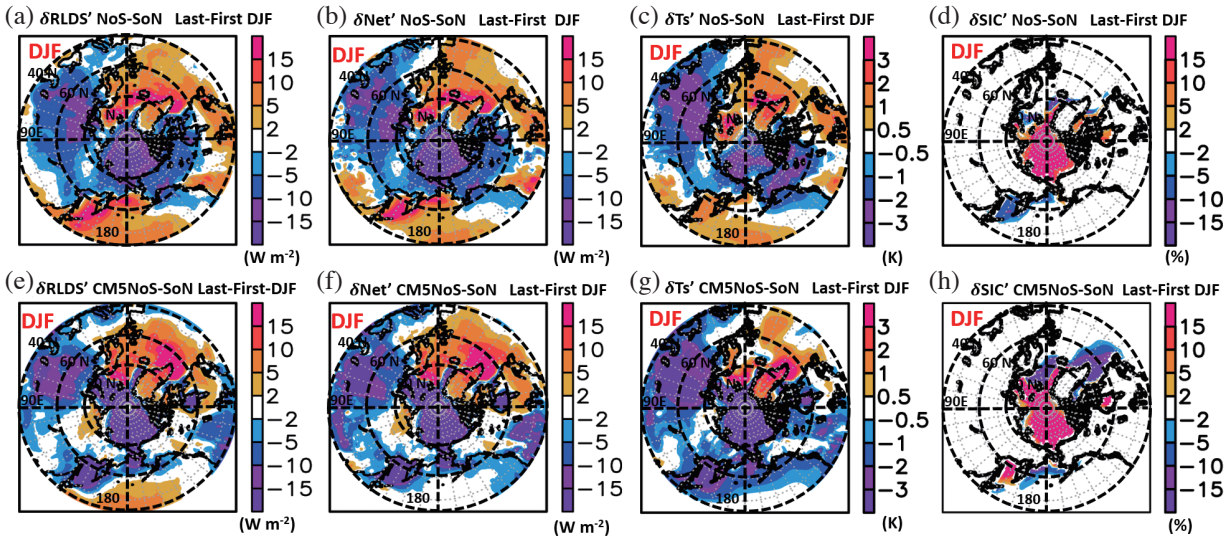

Fig. 6. The difference between falling ice radiative effects (FIREs) off minus FIREs on (NoS - SoN) for December-January-February (DJF) from the changes of annual mean in last 20 years (121 - 140 years) minus first 20 years (1 - 20 years) for (a) downward surface longwave radiation (δRLDS': W m^{-2}), (b) Surface Net flux (δNet': W m^{-2}), (c) Surface skin temperature (δT': K), (d) sea ice concentration (δSIC': %). (e) - (h) Same as (a) - (d) but for CMIP5 multi-model mean (CMIP5-NoS) without FIREs minus SoN. The simulation outputs are from CESM1 experiments of NoS and SoN and CMIP5 models following the CMIP5 1%CO2 scenario for 140 years.

terms of geographical distributions, how FIREs may impact the changes of radiation budgets, skin temperatures and SIC and THK over Arctic oceans and the radiation budgets and land skin temperatures over adjacent areas.

With FIREs included, relative to neglecting falling ice mass, the net flux warming (AELW) dominated by RLDS could be up to 10 - 25 W m^{-2} over much of the Arctic Ocean in the initial warming period. This difference is contributed by increased downward longwave radiation and decreased downward surface shortwave radiation and albedo cooling. The spatial pattern of change in radiative properties, SIC, sea ice thickness and Ts across the Arctic Ocean with global warming is typically more sensitive in SoN relative to NoS. The mass changes from snow on sea ice area have less impacts on sea ice changes, indicating the importance of energy adjustment rather than that of mass balance on the sea ice simulations, which is similar to what has been found for present-day simulation (Li et al. 2019).

We examined the geographical distributions of changes in terms of annual-mean, winter (DJF) and summer (JJA) means of radiative fluxes (RLDS, RSDS, RSUS, and Net Flux), Ts, SIC, and THK for the initial stage (years 1 - 20), middle stage (years 61 - 80), and warmest stage (years 121 - 140). The changes in annual-mean differences (NoS minus SoN) of SIC and sea ice thickness from the first 20-year to middle 20-year are small, while those of SIC increase, accompanied with more sea ice thinning, from the middle to last 20-year, which are associated with less RLDS and AELW over the sea ice-covered regions. This is also the case in winter (DJF). The increased warming restricts the growth of area and thickness of sea ice, leading to a faster melting rate in sea-ice concentration during the 140-year integration, compared to the NoS simulation. During summer (JJA), the situation is more complex, i.e., when FIRE is included, decreased surface albedo in conjunction to decreased downward SW could result in decreasing surface SW cooling (because of smaller albedo) in sea ice-covered regions. If the downward LW flux is sufficiently large so that the net radiative flux increases, it results in retreats of sea ice and thinning of sea ice. This albedo cooling effect also partially offsets the increased amount of LW heating due to FIREs, making sea ice changes more complex in summer, as well as in spring and fall, resulting in lagged sea ice response.

The sea ice thickness seasonal changes in DJF and JJA between the last 20-year and first 20-year are similar to the SIC changes, showing more retreats of sea ice and more thinning in DJF than in JJA. During the melting seasons, the ocean-only area averages of SIC values over the belts 60 - 90°N indicate that the CESM1-SoN simulation shows a faster long-term sea ice melting rate than the CESM1-NoS simulation without differences in snow on sea ice area during the 140 years.

We also demonstrated that net downward radiation reduction changes due to FIREs between the last and first warming stages over sea-ice covered area and adjacent areas between 40 and 90°N are similar to those in CMIP5-NoS minus SoN during winter, but less so for annual mean and

during summer. The geographical pattern of SIC and sea ice thickness changes in NoS minus SoN with progressive global warming largely matches that of CMIP5-NoS minus SoN. It is found that in the last 20 years, with FIREs, the SIC decreases over 15% with 20 - 60 cm thinning compared to NoS and CMIP5-NoS. In DJF, the tendency changes (last 20 years minus first 20 years) for NoS - SoN of radiative fluxes, Ts and skin temperatures are similar to those of CMIP5-NoS minus SoN except for opposite trend of changes over the far north-east Pacific Ocean regions. Compared to NoS and CMIP5-NoS, with FIREs, the model projects stronger warming tendency of approximately 3 - 8°K over Europe and north of 40°N, between longitudes of 30 - 90°E as well as decreased south-north Ts gradients over Pacific and Atlantic oceans around 50°N.

As discussed above, geographic patterns of change are similar between CMIP5-NoS and NoS. This resemblance implies that an improper representation of the falling ice-radiation interaction contributes, at least partially, to differences in the simulation of climate change over the Arctic Ocean and adjacent areas under the CO_2-driven global warming. Shown in Fig. A8 is Ocean only monthly mean time series which indicates that with FIREs, the contributions of net surface flux (Fig. 1c) is mainly from surface downward longwave flux (Fig. A8a) for all seasons. The associated surface downward shortwave flux (Fig. A8b) and surface reflected shortwave flux (Fig. A8c) also play a non-negligible role during the summer season. In these CESM1 simulations, it appears that inclusion of FIREs drives faster sea ice melting and thinning over the entire Arctic oceans, associated with enhanced longwave warming and warmer Ts.

The results presented in this study have shown that including FIREs is an important process for simulating the changes of radiative balance and sea-ice concentration over the Arctic Ocean under progressive global warming. Our results suggest that FIRE is potentially an important process with substantial effects on simulated energy budgets and sea ice formation and retreat although other physical-dynamical processes not examined in this study may play a substantial role. Nevertheless, such a physics-based improvement, if applied across all models, would increase our confidence on the projections of regional changes affecting climate feedbacks such as the albedo feedback. Inferring the results found in this study to each CMIP5 model, however, is difficult because tests with each of these CMIP5 models are needed, which is beyond the scope of this study, in order to determine whether the enhanced dynamic and hydrological responses to CO_2-driven warming is robust for all CMIP5 models.

Finally, we are aware that FIRE is one of many dominant processes in model response to the climate changes in the Arctic. However, given the reduction in model-observation discrepancy of 39 - 66% with the inclusion of FIREs for the present-day climate of the Arctic reported in Li et al. (2019), we believe that excluding FIREs is a critical shortcoming for most state-of-the-art GCMs used to project the future state of Arctic climate and sea ice coverage. Given that FIRE is already included in more CMIP Phase 6 (CMIP6; Eyring et al. 2016) models, this study provides motivation for all other models to address an easily understood physical process that may cause notable biases in climate simulations, which will lead to improvement of climate projection across the majority of climate models used in an upcoming Intergovernmental Panel on Climate Change (IPCC) assessment report.

Acknowledgements We thank the Editor and all reviewers, who provided us helpful comments on earlier versions of this manuscript. The contribution by JLL to this study was carried out on behalf of the Jet Propulsion Laboratory, California Institute of Technology, under contracts of NASA Making Earth System Data Records for Use in Research Environments (MEaSUREs) programs with the National Aeronautics and Space Administration (NASA).

REFERENCES

Barnes, E. A. and J. A. Screen, 2015: The impact of Arctic warming on the midlatitude jet-stream: Can it? Has it? Will it? *WIREs Clim. Change*, **6**, 277-286, doi: 10.1002/wcc.337. [Link]

Bintanja, R. and F. M. Selten, 2014: Future increases in Arctic precipitation linked to local evaporation and sea-ice retreat. *Nature*, **509**, 479-482, doi: 10.1038/nature13259. [Link]

Boisvert, L. N. and J. C. Stroeve, 2015: The Arctic is becoming warmer and wetter as revealed by the Atmospheric Infrared Sounder. *Geophys. Res. Lett.*, **42**, 4439-4446, doi: 10.1002/2015GL063775. [Link]

Cesana, G., J. E. Kay, H. Chepfer, J. M. English, and G. de Boer, 2012: Ubiquitous low-level liquid-containing Arctic clouds: New observations and climate model constraints from CALIPSO-GOCCP. *Geophys. Res. Lett.*, **39**, L20804, doi: 10.1029/2012GL053385. [Link]

Cesana, G., D. E. Waliser, X. Jiang, and J.-L. F. Li, 2015: Multimodel evaluation of cloud phase transition using satellite and reanalysis data. *J. Geophys. Res.*, **120**, 7871-7892, doi: 10.1002/2014JD022932. [Link]

Eyring, V., S. Bony, G. A. Meehl, C. A. Senior, B. Stevens, R. J. Stouffer, and K. E. Taylor, 2016: Overview of the Coupled Model Intercomparison Project Phase 6 (CMIP6) experimental design and organization. *Geosci. Model Dev.*, **9**, 1937-1958, doi: 10.5194/gmd-9-1937-2016. [Link]

Francis, J. A. and S. J. Vavrus, 2012: Evidence linking Arctic amplification to extreme weather in midlatitudes. *Geophys. Res. Lett.*, **39**, L06801, doi:

10.1029/2012GL051000. [Link]

Gettelman, A. and H. Morrison, 2015: Advanced two-moment bulk microphysics for global models. Part I: Off-line tests and comparison with other schemes. *J. Clim.*, **28**, 1268-1287, doi: 10.1175/JCLI-D-14-00102.1. [Link]

Gettelman, A., X. Liu, S. J. Ghan, H. Morrison, S. Park, A. J. Conley, S. A. Klein, J. Boyle, D. L. Mitchell, and J.-L. F. Li, 2010: Global simulations of ice nucleation and ice supersaturation with an improved cloud scheme in the Community Atmosphere Model. *J. Geophys. Res.*, **115**, D18216, doi: 10.1029/2009JD013797. [Link]

Gettelman, A., H. Morrison, S. Santos, P. Bogenschutz, and P. M. Caldwell, 2015: Advanced two-moment bulk microphysics for global models. Part II: Global model solutions and aerosol-cloud interactions. *J. Clim.*, **28**, 1288-1307, doi: 10.1175/JCLI-D-14-00103.1. [Link]

Horvat, C. and E. Tziperman, 2018: Understanding melting due to ocean eddy heat fluxes at the edge of sea-ice floes. *Geophys. Res. Lett.*, **45**, 9721-9730, doi: 10.1029/2018GL079363. [Link]

Jacob, T., J. Wahr, W. T. Pfeffer, and S. Swenson, 2012: Recent contributions of glaciers and ice caps to sea level rise. *Nature*, **482**, 514-518, doi: 10.1038/nature10847. [Link]

Karlsson, J. and G. Svensson, 2013: Consequences of poor representation of Arctic sea-ice albedo and cloud-radiation interactions in the CMIP5 model ensemble. *Geophys. Res. Lett.*, **40**, 4374-4379, doi: 10.1002/grl.50768. [Link]

Kay, J. E., T. L'Ecuyer, A. Gettelman, G. Stephens, and C. O'Dell, 2008: The contribution of cloud and radiation anomalies to the 2007 Arctic sea ice extent minimum. *Geophys. Res. Lett.*, **35**, L08503, doi: 10.1029/2008GL033451. [Link]

Kay, J. E., M. M. Holland, and A. Jahn, 2011: Inter-annual to multi-decadal Arctic sea ice extent trends in a warming world. *Geophys. Res. Lett.*, **38**, L15708, doi: 10.1029/2011GL048008. [Link]

Kirchmeier-Young, M. C., F. W. Zwiers, and N. P. Gillett, 2017: Attribution of extreme events in Arctic sea ice extent. *J. Clim.*, **30**, 553-571, doi: 10.1175/JCLI-D-16-0412.1. [Link]

Kjeldsen, K. K., N. J. Korsgaard, A. A. Bjørk, S. A. Khan, J. E. Box, S. Funder, N. K. Larsen, J. L. Bamber, W. Colgan, M. van den Broeke, M.-L. Siggaard-Andersen, C. Nuth, A. Schomacker, C. S. Andresen, E. Willerslev, and K. H. Kjær, 2015: Spatial and temporal distribution of mass loss from the Greenland Ice Sheet since AD 1900. *Nature*, **528**, 396-400, doi: 10.1038/nature16183. [Link]

Koenigk, T., A. Devasthale, and K.-G. Karlsson, 2014: Summer Arctic sea ice albedo in CMIP5 models. *Atmos. Chem. Phys.*, **14**, 1987-1998, doi: 10.5194/acp-14-1987-2014. [Link]

Kurtz, N. T. and T. Markus, 2012: Satellite observations of Antarctic sea ice thickness and volume. *J. Geophys. Res.*, **117**, C08025, doi: 10.1029/2012JC008141. [Link]

Kwok, R. and G. F. Cunningham, 2008: ICESat over Arctic sea ice: Estimation of snow depth and ice thickness. *J. Geophys. Res.*, **113**, C08010, doi: 10.1029/2008JC004753. [Link]

Li, J.-L. F., M. Richardson, Y. Hong, W.-L. Lee, Y.-H. Wang, J.-Y. Yu, E. Fetzer, G. Stephens, and Y. Liu, 2017: Improved simulation of Antarctic sea ice due to the radiative effects of falling snow. *Environ. Res. Lett.*, **12**, 084010, doi: 10.1088/1748-9326/aa7a17. [Link]

Li, J.-L. F., M. Richardson, W.-L. Lee, E. Fetzer, G. Stephens, J. Jiang, Y. Hong, Y.-H. Wang, J.-Y. Yu, and Y. Liu, 2019: Potential faster Arctic sea ice retreat triggered by snowflakes' greenhouse effect. *The Cryosphere*, **13**, 969-980, doi: 10.5194/tc-13-969-2019. [Link]

Massonnet, F., T. Fichefet, H. Goosse, C. M. Bitz, G. Philippon-Berthier, M. M. Holland, and P.-Y. Barriat, 2012: Constraining projections of summer Arctic sea ice. *The Cryosphere*, **6**, 1383-1394, doi: 10.5194/tc-6-1383-2012. [Link]

Massonnet, F., M. Vancoppenolle, H. Goosse, D. Docquier, T. Fichefet, and E. Blanchard-Wrigglesworth, 2018: Arctic sea-ice change tied to its mean state through thermodynamic processes. *Nat. Clim. Change*, **8**, 599-603, doi: 10.1038/s41558-018-0204-z. [Link]

Mori, M., Y. Kosaka, M. Watanabe, B. Taguchi, H. Nakamura, and M. Kimoto, 2019: Reply to: Is sea-ice-driven Eurasian cooling too weak in models? *Nat. Clim. Change*, **9**, 937-939, doi: 10.1038/s41558-019-0636-0. [Link]

Morrison, H. and A. Gettelman, 2008: A new two-moment bulk stratiform cloud microphysics scheme in the Community Atmosphere Model, Version 3 (CAM3). Part I: Description and numerical tests. *J. Clim.*, **21**, 3642-3659, doi: 10.1175/2008JCLI2105.1. [Link]

Rigor, I. G. and J. M. Wallace, 2004: Variations in the age of Arctic sea-ice and summer sea-ice extent. *Geophys. Res. Lett.*, **31**, L09401, doi: 10.1029/2004GL019492. [Link]

Shiklomanov, N. I., D. A. Streletskiy, T. B. Swales, and V. A. Kokorev, 2017: Climate change and stability of urban infrastructure in Russian permafrost regions: Prognostic assessment based on GCM climate projections. *Geogr. Rev.*, **107**, 125-142, doi: 10.1111/gere.12214. [Link]

Smedsrud, L. H., M. H. Halvorsen, J. C. Stroeve, R. Zhang, and K. Kloster, 2017: Fram Strait sea ice export

variability and September Arctic sea ice extent over the last 80 years. *The Cryosphere*, **11**, 65-79, doi: 10.5194/tc-11-65-2017. [Link]

Smith, L. C. and S. R. Stephenson, 2013: New Trans-Arctic shipping routes navigable by midcentury. *Proc. Natl. Acad. Sci.*, **110**, E1191-E1195, doi: 10.1073/pnas.1214212110. [Link]

Stroeve, J. C., V. Kattsov, A. Barrett, M. Serreze, T. Pavlova, M. Holland, and W. N. Meier, 2012: Trends in Arctic sea ice extent from CMIP5, CMIP3 and observations. *Geophys. Res. Lett.*, **39**, L16502, doi: 10.1029/2012GL052676. [Link]

Tan, I., T. Storelvmo, and M. D. Zelinka, 2016: Observational constraints on mixed-phase clouds imply higher climate sensitivity. *Science*, **352**, 224-227, doi: 10.1126/science.aad5300. [Link]

Taylor, K. E., R. J. Stouffer, and G. A. Meehl, 2012: An overview of CMIP5 and the experiment design. *Bull. Amer. Meteorol. Soc.*, **93**, 485-498, doi: 10.1175/BAMS-D-11-00094.1. [Link]

Tietsche, S., D. Notz, J. H. Jungclaus, and J. Marotzke, 2011: Recovery mechanisms of Arctic summer sea ice. *Geophys. Res. Lett.*, **38**, L02707, doi: 10.1029/2010GL045698. [Link]

APPENDIX

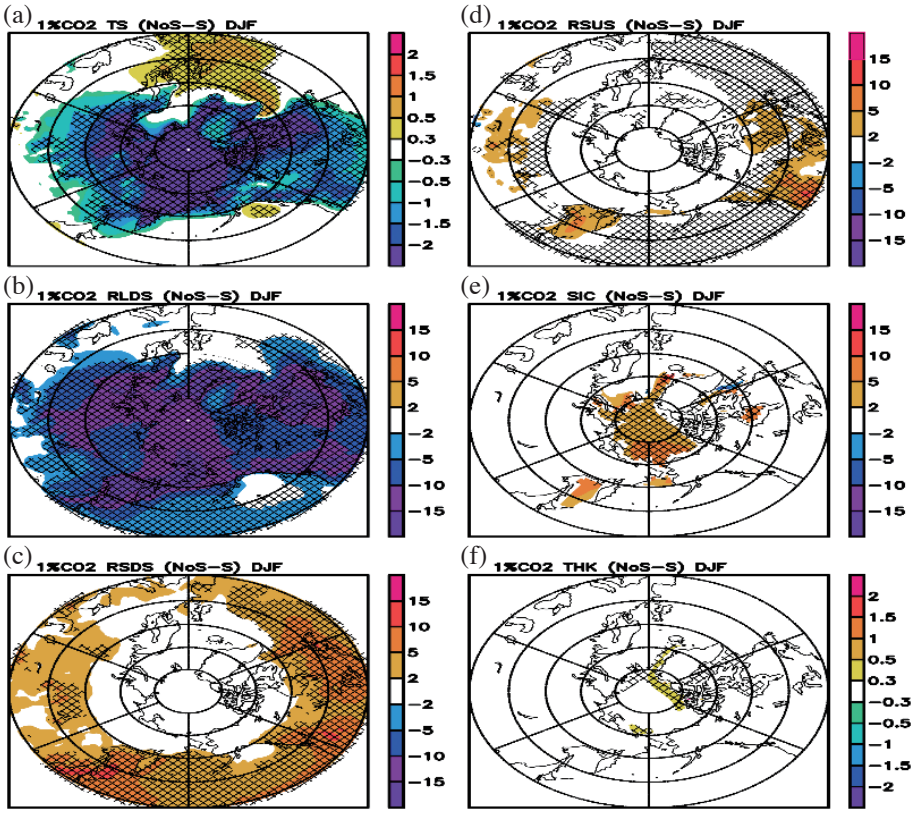

Fig. A1. Difference between CESM1 falling ice radiative effects (FIRE) off minus on (NoS - S) for December-January-February (DJF) mean for 140 years in 1%CO2 scenario for (a) skin temperature (TS: K), (b) same as (a) but for downward surface longwave radiation (RLDS: W m^{-2}), (c) same as (a) but for downward surface shortwave radiation (RSDS: W m^{-2}), (d) same as (a) but for upward surface shortwave radiation (RSUS: W m^{-2}), (e) same as (a) but for sea ice concentration (SIC: %), (f) same as (a) but for sea ice thickness (THK: cm).

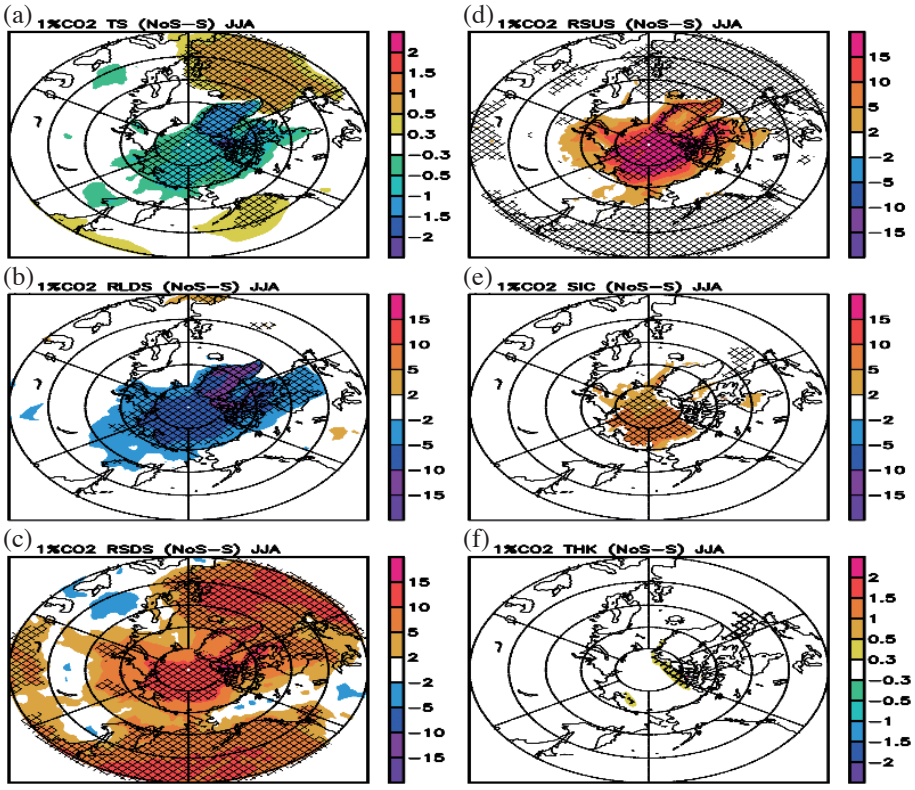

Fig. A2. Same as Fig. A1 but for June-July-August (JJA).

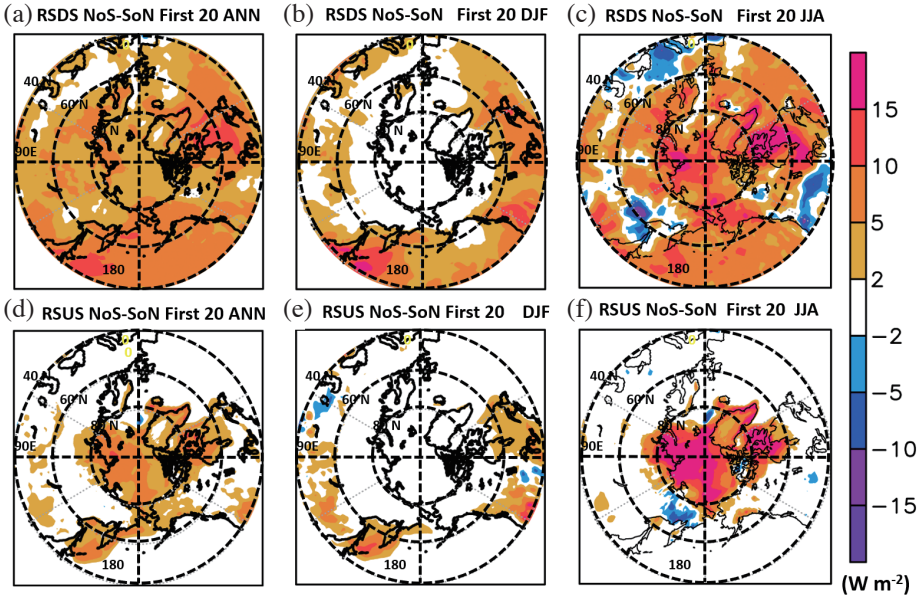

Fig. A3. Difference between CESM1 falling ice radiative effects (FIRE) off minus on (NoS - SoN) for first 20 years (1 - 20 years) in 1%CO2 scenario for downward surface shortwave radiation (RSDS': W m^{-2}) for (a) annual mean, (b) for DJF, (c) for JJA for downward surface shortwave radiation (RSDS': W m^{-2}). (d) - (f) Same as (a) - (c) but for upward surface shortwave radiation (RSUS': W m^{-2}).

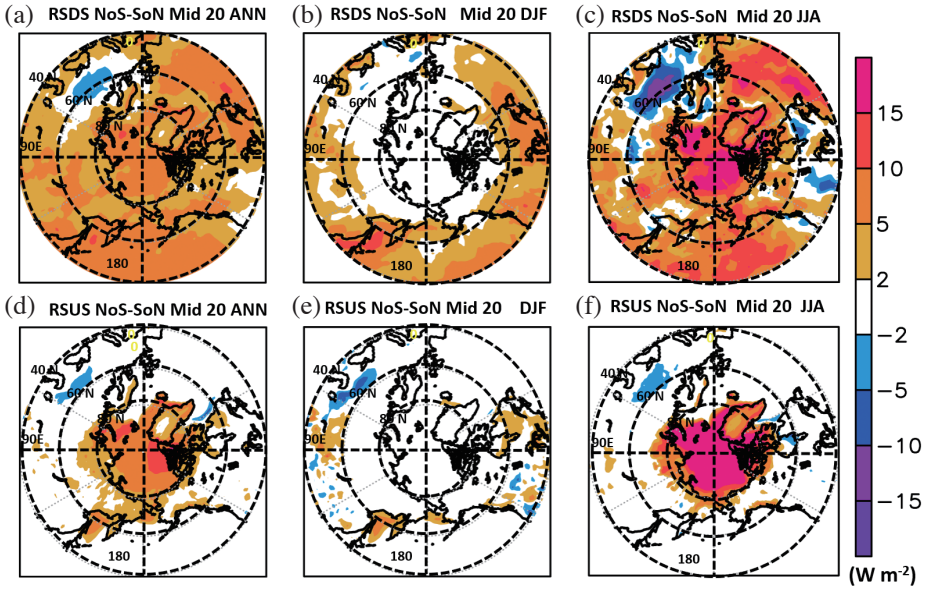

Fig. A4. Same as Fig. A3 but for middle 20 years (61 - 80 years).

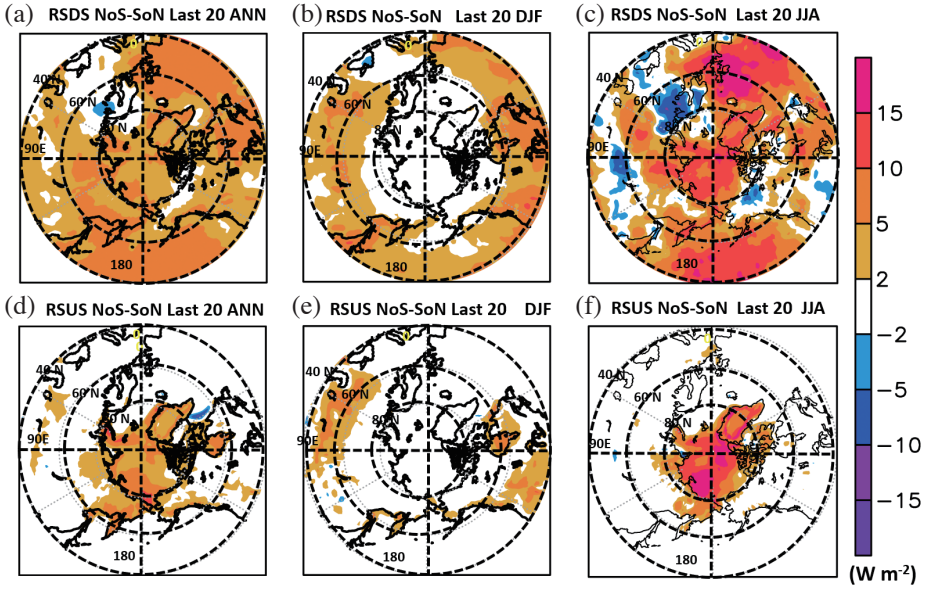

Fig. A5. Same as Fig. A3 but for the last 20 years (121 - 140 years).

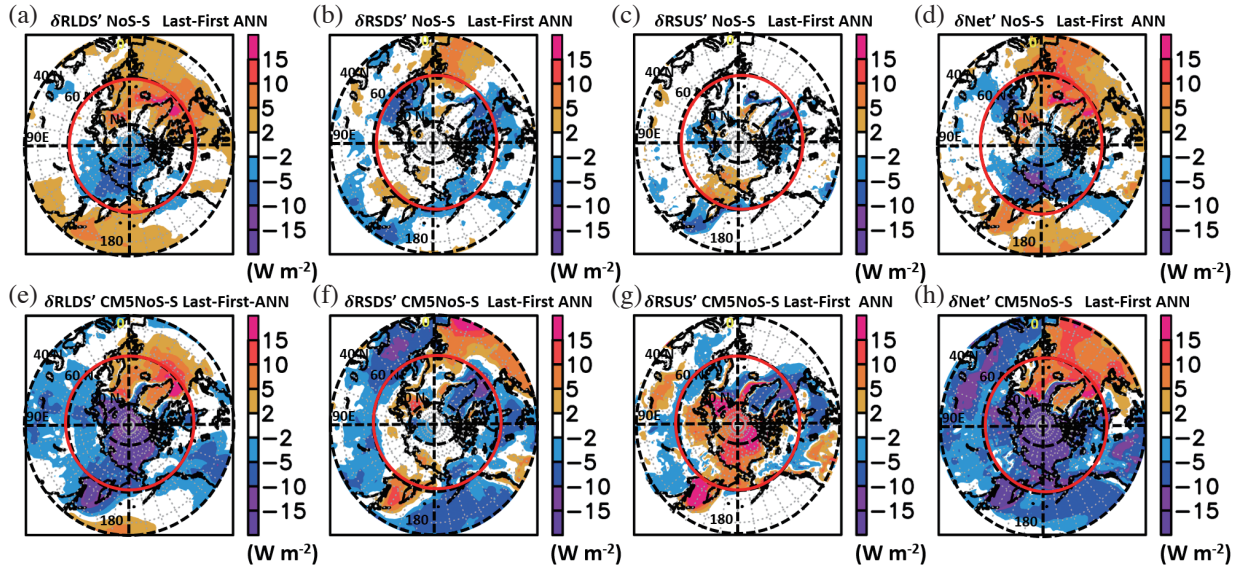

Fig. A6. Annual mean for the changes between mean of the last 20 years and first 20 years in 1%CO2 scenario (i.e., the last 20 years minus the first 20 years) from NoS minus SoN for (a) Surface downward longwave radiation, δRLDS', (b) Surface downward shortwave radiation, δRSDS', (c) Surface upward shortwave radiation, δRSUS', (d) Surface net flux, δNet'. (e) - (h) Same as (a) - (d) but for CMIP5 multi-model mean (CMIP5-NoS).

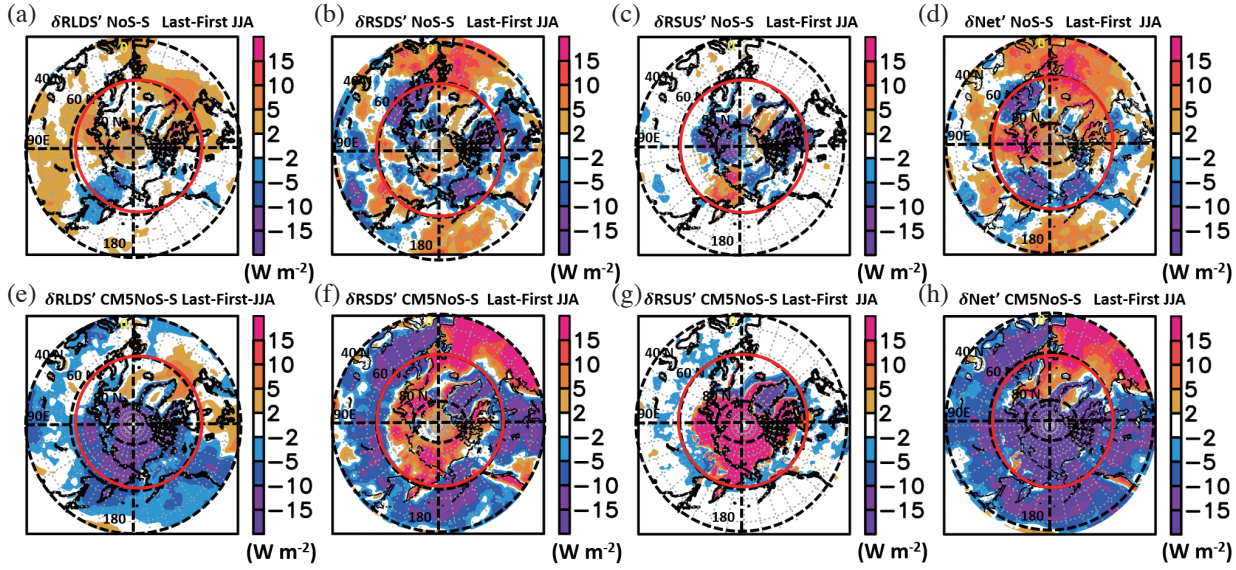

Fig. A7. As in Fig. A6, but for June-July-August (JJA).

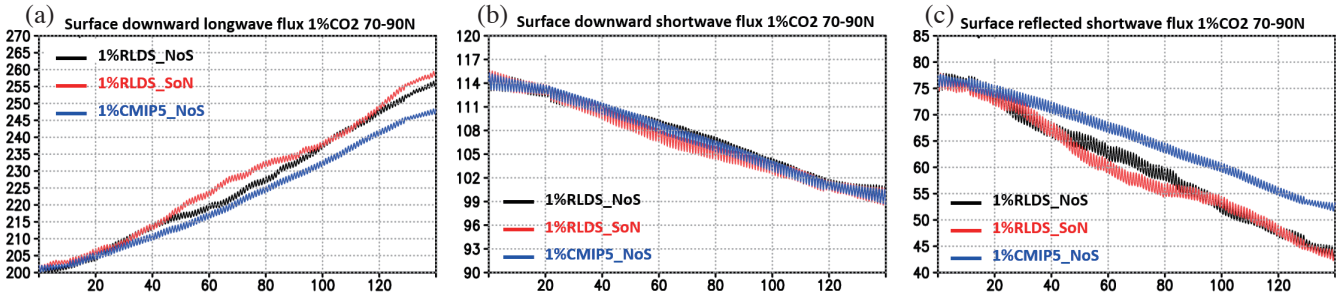

Fig. A8. Ocean only monthly mean time series of (a) surface downward longwave flux (W m-2) FIREs off (NoS: black line), FIREs on (SoN: red line) and CMIP5 multi-model mean (CMIP5-NoS) without FIREs averaged over the latitude belts 70 - 90°N under 1%CO2 per year for 140 years. (b) Same as (a) but for surface downward shortwave flux (W m-2); (c) same as (a) but for surface reflected shortwave flux (W m-2).